Curr Radiol Rep (2017) 5:60
DOI 10.1007/s40134-017-0251-7

PEDIATRICS (L AVERILL, SECTION EDITOR)

Neuroimaging of Pediatric Metabolic Disorders with Emphasis on Diffusion-Weighted Imaging and MR Spectroscopy: A Pictorial Essay

Kofi-Buaku Atsina[1] · Lauren W. Averill[2,3] · Vinay V. R. Kandula[3]

Published online: 15 September 2017

Abstract
Purpose of Review Although individually rare, metabolic brain disorders together account for significant disease burden in infants and children. MRI evaluation of these disorders is daunting, but using a pattern-based approach is helpful. Here we present 10 of the most commonly encountered metabolic brain disorders, highlighting specific features on DWI and MR spectroscopy that help narrow the differential diagnosis.
Recent findings A number of metabolic diseases result in elevated lactate at 1.3 ppm in affected areas. Other metabolite derangements, though, are more helpful in determining the underlying disease. MR spectroscopy showing elevated glycine at 3.55 ppm indicates nonketotic hyperglycinemia, while markedly elevated NAA at 2.0 ppm is characteristic of Canavan disease. NAA will be low in diseases causing neuronal loss, and can be even absent in Alexander disease. Absent or severely low creatine at 3.0 ppm is specific for the family of creatine deficiency syndromes. The pattern of restricted diffusion seen with DWI can also point to a specific diagnosis, especially with brainstem and cerebellar white matter involvement seen with maple syrup urine disease. Additionally, both MR spectroscopy and DWI can be used to follow disease progression or response to therapy.
Summary DWI and MR spectroscopy are useful adjuncts to anatomic brain imaging in the evaluation of pediatric metabolic brain disorders.

Keywords Metabolic · MRI · Pediatric · Brain · Diffusion-weighted imaging · MR spectroscopy

Introduction

Although each individual metabolic brain disorder is rare, together they account for a significant burden of disease in infants and children, and will present to general radiologists as well as subspecialist pediatric imagers. Piecing together age at onset, symptoms, and acuity of presentation with varied imaging findings into a targeted differential diagnosis is daunting, even for pediatric neuroradiologists. This task, though, is important in the age of genomics, with more and more causative genes identified with pediatric metabolic disorders. A tailored radiology report can focus the initial workup on specific laboratory and genetic testing, saving both expense and time as well as allowing for prompt intervention. In certain disorders, such as maple syrup urine disease, immediate targeted therapy directed by imaging findings is critical to patient survival.

In addition to conventional anatomic magnetic resonance imaging (MRI), we find that features on diffusion-weighted imaging (DWI) and MR spectroscopy are especially useful in pinpointing the most likely metabolic brain disorder. Single-voxel MR spectroscopy utilizing short (35 ms) and intermediate-to-long echo times (144 or 288 ms) can be performed at 1.5 or 3 Tesla, adding approximately 5 min to the examination. Although

This article is part of the Topical Collection on *Pediatrics*.

✉ Vinay V. R. Kandula
vinay.kandula@nemours.org

[1] Department of Radiology, Sidney Kimmel Medical College, Thomas Jefferson University, Philadelphia, PA, USA

[2] Sidney Kimmel Medical College, Thomas Jefferson University, Philadelphia, PA, USA

[3] Medical Imaging, Nemours Children's Health System, Alfred I. duPont Hospital for Children, 1600 Rockland Road, Wilmington, DE 19803, USA

complex analysis can be performed, DWI and MR spectroscopy can be incorporated into routine MRI interpretation using a pattern-based approach. In this article, we present 10 of the most common pediatric metabolic brain disorders that we have encountered over the past 10 years, focusing on the added utility of DWI and MR spectroscopy.

Maple Syrup Urine Disease

Maple syrup urine disease (MSUD) is a rare autosomal-recessive disorder caused by deficiency of the branched-chain α-ketoacid dehydrogenase complex leading to the buildup of branched-chain amino acids or BCAAs (leucine, isoleucine and valine) and branched-chain α-ketoacids (BCKAs), which are toxic byproducts. Accumulation of BCKAs in the serum, cerebrospinal fluid, and urine gives rise to the characteristic maple syrup odor [1]. It is estimated to affect approximately 1/180,000–1/185,000 infants worldwide; [2, 3••] however, the incidence is much higher among the Old Order Mennonite communities [4, 5].

Four phenotypes have been described. The most common phenotype is the classic form, in which early signs and symptoms can be detected within the first 12–24 h after birth, but typically during the first 4–7 days. The antenatal and birth histories are usually unremarkable. Symptoms are progressive over the next few days ranging from irritability, dystonia, opisthotonus, and poor feeding to lethargy and seizures, to deepening encephalopathy, intermittent apnea, and eventual death [2, 6]. The intermediate form of this disease is characterized by elevated BCKAs, and normal or elevated BCAAs, and usually precipitated by a stressor such as infection. Individuals progress from normal development to progressive mental retardation and developmental delay [2, 7]. Other phenotypes such as intermittent and thiamine responsive type are rare [2].

Prompt imaging diagnosis may be critical for patients with MSUD, since appropriate therapy needs to be implemented immediately. On computed tomography (CT), there is diffuse symmetric edema not sparing the cerebellum and brainstem. In classic MSUD, the infratentorial white matter is much more affected than supratentorial white matter. There is involvement of cerebellar white matter, dorsal brainstem, cerebral peduncles, internal capsules, thalami, and globus pallidi. The pyramidal and tegmental tracts are also affected. On T2-weighted MRI sequences, there is usually generalized diffuse edema, with localized more severe edema in the deep cerebellar white matter, dorsal brainstem, and corticospinal tracts (Fig. 1). DWI is the most helpful sequence, demonstrating restricted diffusion in the afore-mentioned affected areas due to cytotoxic edema [8–11]. On MR spectroscopy, there is abnormal presence of BCAAs and BCKAs at 0.9 ppm and elevated lactate levels. N-acetylaspartic acid (NAA) is decreased. Restricted diffusion on MR imaging as well as MR spectroscopy changes are reversible with treatment; T2 changes lag behind [11].

Nonketotic Hyperglycinemia (Glycine Encephalopathy)

Nonketotic hyperglycinemia (NKH) is an autosomal-recessive disorder of glycine metabolism characterized by a defect in the glycine cleavage enzyme system resulting in the accumulation of glycine in plasma and cerebrospinal fluid causing severe encephalopathy [12, 13]. The glycine cleavage enzyme system is composed of four proteins encoded by genes on chromosomes 9p23–24, 3q21.1–21.2, 16q24, and 7q31–32 [13].

At least four phenotypes have been described. The neonatal and most common phenotype is a severe form that presents with lethargy, hypotonia, myoclonic jerks, seizures, coma, and episodes of apnea requiring ventilator support. A milder form presents during infancy (after 6 months), and is characterized by mild mental retardation triggered by febrile illness, following normal initial development. Patients may present with episodes of delirium, agitation, chorea, and vertical gaze palsy. The late-onset form has a variable neurological presentation, which may be characterized by spasticity, optic atrophy, and neurological degeneration. A transient form has been described which has a similar phenotypic expression as the neonatal severe form [14].

NKH is characterized by vacuolating spongy myelinopathy, affecting formed myelin sheaths or delaying myelination [15•, 16]. In early forms, the disease tends to be confined to myelinated white matter tracts already formed at the time of birth, such as dorsal pons, midbrain, cerebellar white matter, posterior limb of the internal capsule, thalami, and globus pallidi [13, 17]. On MRI, restricted diffusion with accompanying high T2 and fluid-attenuated inversion recovery (FLAIR) signal characterize these areas (Fig. 2) [13, 15•, 16, 18]. This pattern of restricted diffusion is similar to that of MSUD; however, the T2/FLAIR signal hyperintensity is more extensive in MSUD [13]. In the neonatal form, patients may present with supra- and infratentorial atrophy, ventriculomegaly [19], porencephaly [17], and thinning of the corpus callosum [16] or complete/partial callosal agenesis [15•, 20]. MR spectroscopy demonstrates an increased glycine peak at 3.55 ppm, which is best identified on a long echo time, [15•, 21–23] as short echo time MR spectroscopy also yields an elevated peak of myo-inositol at the same location [15•, 23].

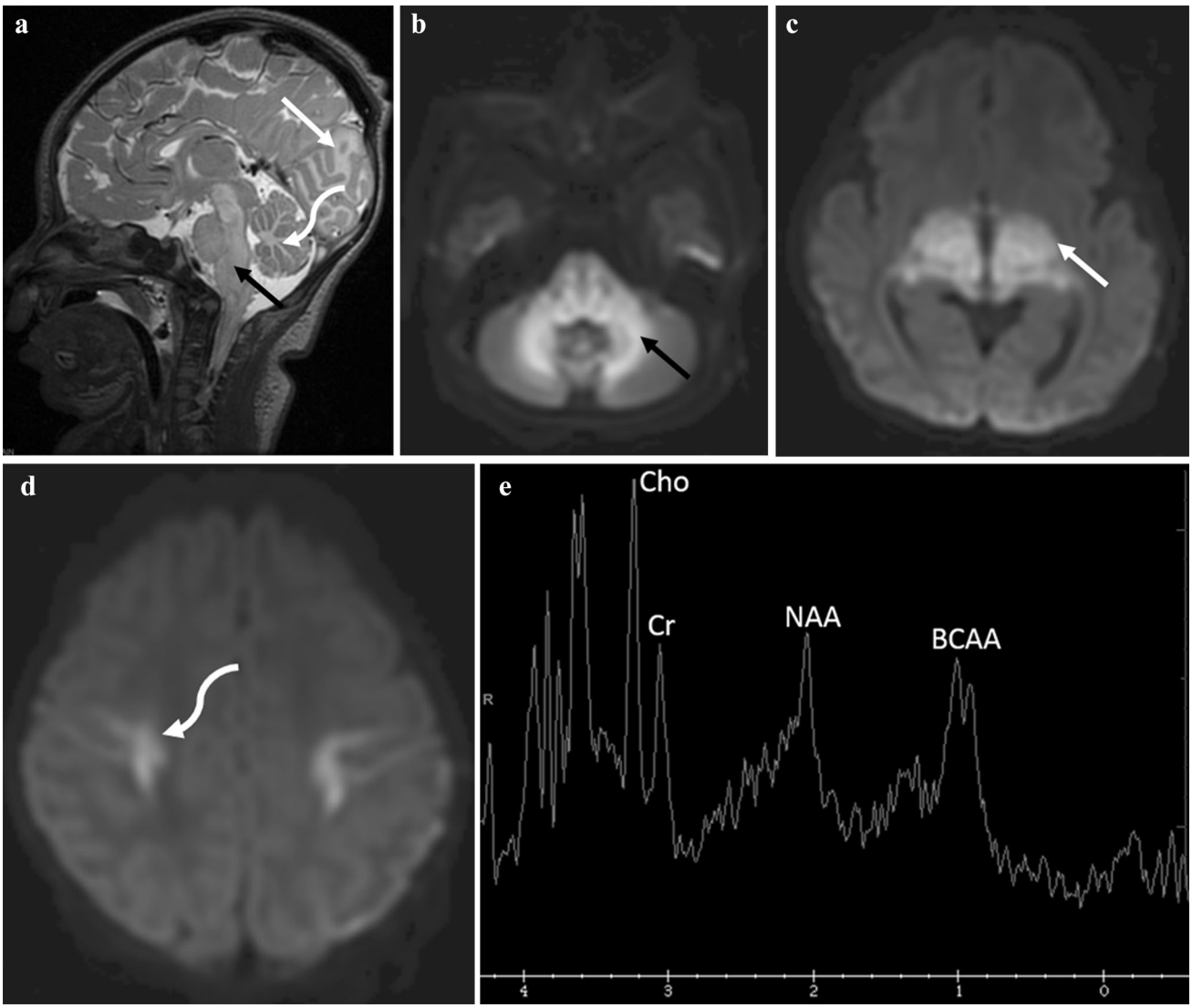

Fig. 1 Maple syrup urine disease. A sagittal T2-weighted image (**a**) demonstrates abnormal hyperintensity in the dorsal brainstem (*black arrow*), cerebellar white matter (*curved white arrow*), and occipital white matter (*straight white arrow*). Axial diffusion-weighted images at 3 different levels (**b**–**d**) show severely restricted diffusion due to intramyelinic edema involving the cerebellar white matter and middle cerebellar peduncles (*black arrow*, **b**), brainstem, midbrain, cerebral peduncles, bilateral thalami (*white arrow*, **c**), anterior and posterior limbs of the internal capsules, and the corticospinal tracts extending into the centrum semiovale (*curved arrow*, **d**). Spectroscopy with TE = 35 ms (**e**) shows an abnormal large peak seen at 0.9 ppm most consistent with elevated branched-chain amino acids (BCAA). NAA (NAA) at 2.0 ppm and creatine (Cr) at 3.0 ppm are decreased, while choline (Cho) at 3.2 ppm remains normal

Canavan Disease

Canavan disease is an autosomal-recessive spongiform leukodystrophy that is characterized by deficiency of N-acetylaspartoacylase enzyme, which converts NAA into aspartate and acetate in the brain, which is essential for myelin synthesis. Enzyme deficiency results in the accumulation of NAA in white matter, cerebrospinal fluid (CSF), blood, and urine, and results in spongiform myelin degeneration [24–26].

The disease has been most commonly described in the Ashkenazi Jewish population and is most commonly characterized by onset in infancy, with neurodevelopmental delay, or arrest, seizures, macrocephaly, hypotonia, visual impairment, and eventual death in early childhood [24, 26]. Phenotypic variations have, however, been reported with three clinically distinct presentations described: a congenital severe form which is symptomatic at birth or within the first few weeks of life, an infantile form noticeable by 3–6 months with unremarkable

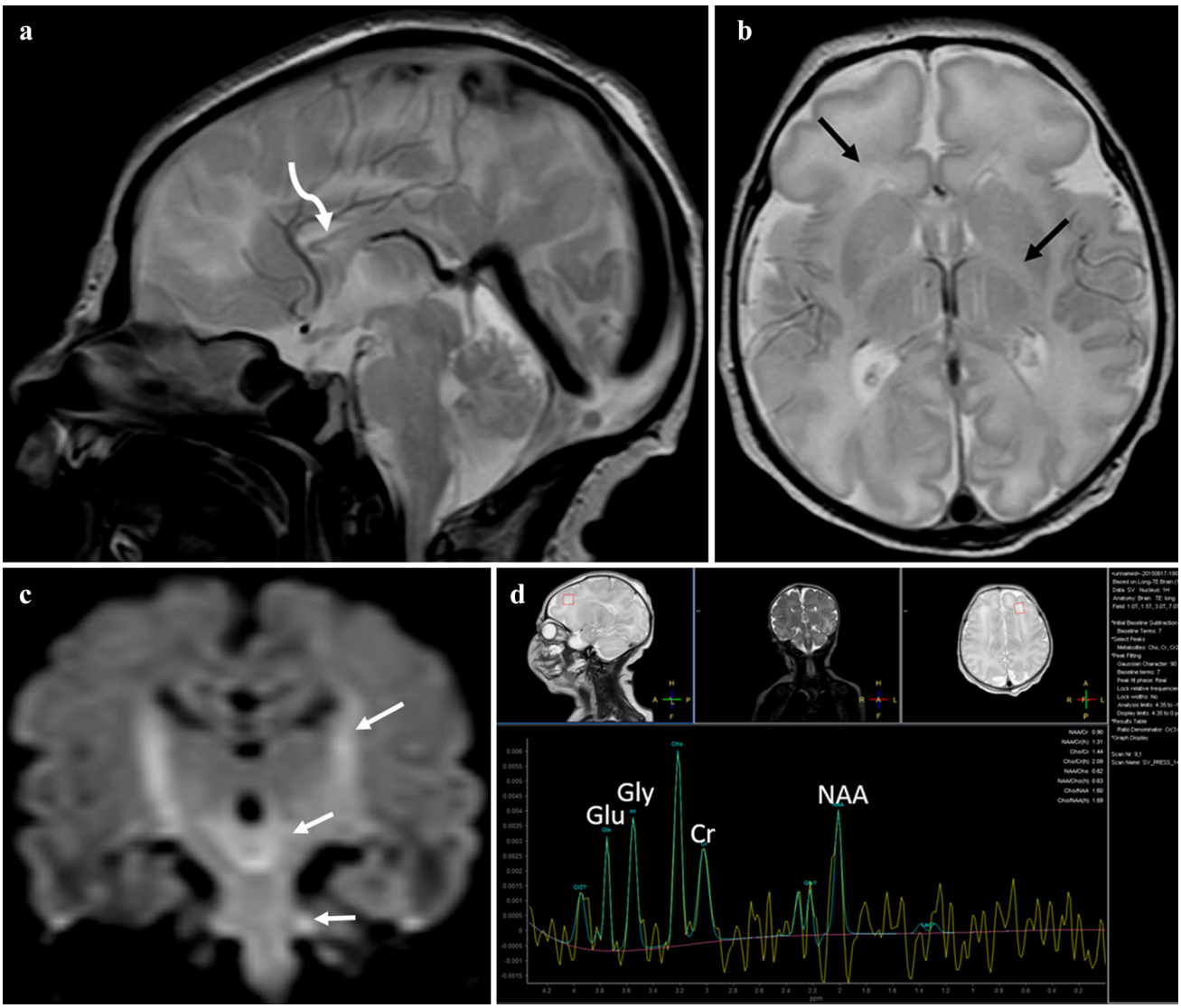

Fig. 2 Nonketotic hyperglycinemia. A sagittal T2-weighted images of the brain (**a**) demonstrate diffuse thinning of the corpus callosum (*curved arrow*). An axial T2-weighted image (**b**) shows global severely delayed myelination with T2 hyperintense white matter edema (*black arrows*) and diffuse volume loss. A coronal diffusion-weighted image (**c**) shows restricted diffusion in the corticospinal tracts, lateral thalami, dorsal brainstem, cerebellar peduncles, and cerebellar white matter probably reflecting vacuolating myelinopathy (*white arrows*). Spectroscopy with TE = 144 ms (**d**) shows an abnormal peak in the white matter and basal ganglia at 3.56 ppm representing an elevated glycine peak (Gly), key to the diagnosis of nonketotic hyperglycinemia. Myo-inositol normally precesses at this frequency as well, but is not seen on long echo times. There is also elevated glutamate (Glu) in the white matter at 3.7 ppm seen with long TE. There is mild decrease in creatine (Cr) and NAA (NAA). The NAA/glycine ratio is low and may represent poor prognosis. There is no evidence of abnormal elevation of lipid or lactate at 1.3 ppm

developmental course in the preceding months, and a juvenile form seen by age 4 or 5 years [25].

Affected infants usually present with megalencephaly [27]. The disease has a predilection for the subcortical U-fibers and white matter initially, and then progresses centripetally to involve the deep white matter, typically sparing the putamen and caudate nucleus [28]. There is symmetrical edematous involvement and vacuolization of the subcortical white matter in both hemispheres, resulting in diffuse hypoattenuation on CT, and T1 hypointense/T2 hyperintense signal on MRI (Fig. 3). As the disease progresses, there is involvement of the external and internal capsules, corpus callosum, deep cerebellar white matter [27], corticospinal tracts, and inferiorly in the brainstem affecting the dorsal and ventral pons [26, 27, 29].

In some instances, affected areas demonstrate restricted or reduced diffusion as evidence of the presence of cytotoxic edema secondary to an acute process; however, this phase lasts for approximately a week or less after damage [26], after which there is gradual progression to increased

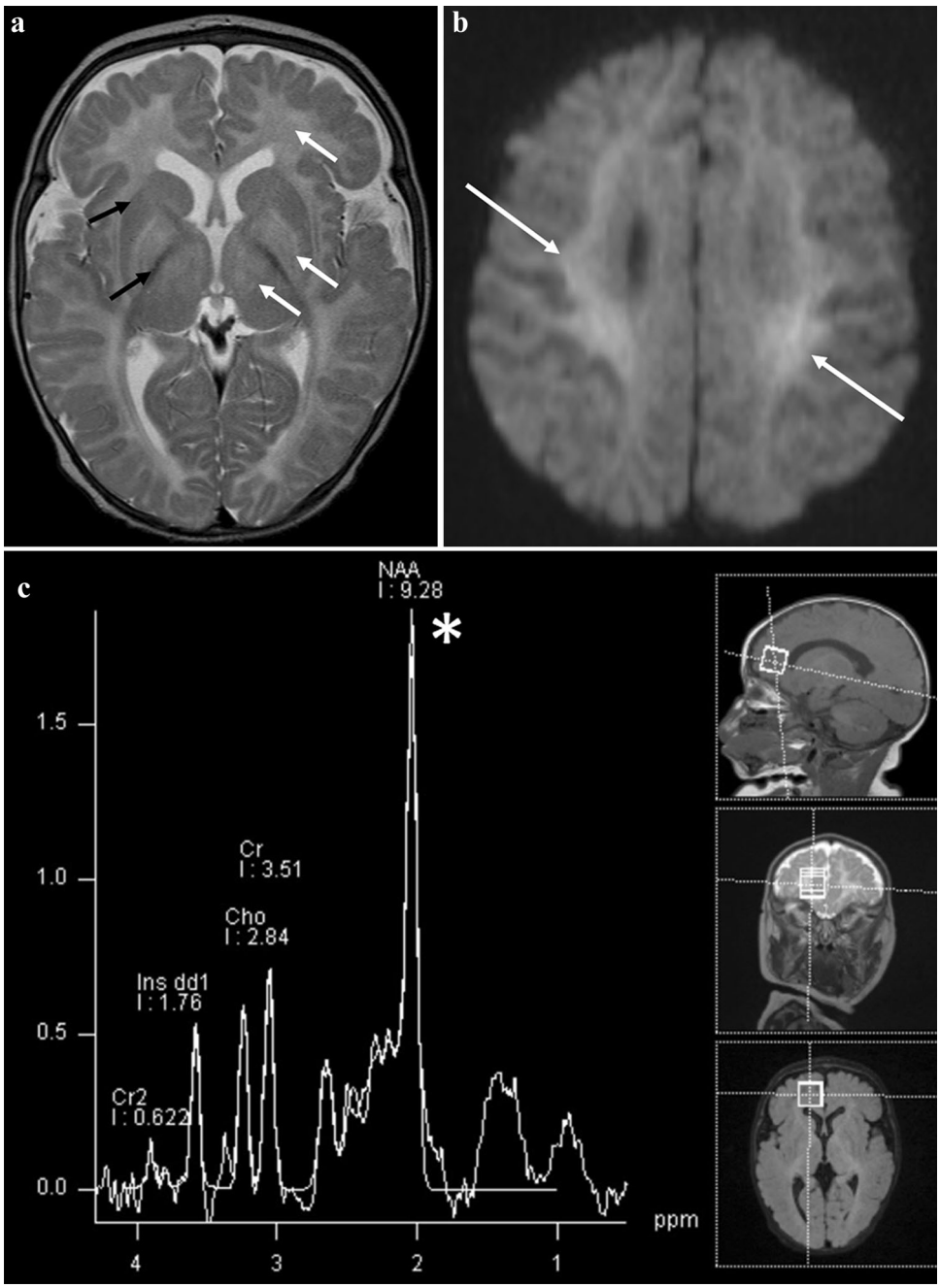

Fig. 3 Canavan disease. An axial T2-weighted image (**a**) shows abnormal high signal in the thalami, globus pallidi, and the entire white matter (*white arrows*). There is relative sparing of the posterior limbs of internal capsules, caudate nuclei, and putamina (*black arrows*). An axial diffusion-weighted image (**b**) demonstrates uniformly restricted diffusion within the abnormal white matter compatible with intramyelinic edema (*arrows*). Spectroscopy with TE = 35 ms (**c**), sampling voxel positioned in the right frontal white matter, shows *markedly* elevated NAA peak at 2.0 ppm (*), considered pathognomonic of Canavan disease. Also note that decreased choline (Cho) and creatine (Cr) peaks, as well as slightly prominent myo-inositol peak (Ins dd1) at 3.54 ppm, labels computer generated

diffusion over time [28]. There is no abnormal enhancement. The markedly elevated NAA seen with MR spectroscopy can be helpful in distinguishing this entity from other leukodystrophies such as Alexander disease. There is also elevation of NAA/creatine and NAA/choline ratios [30••, 31].

Creatine Deficiency Syndromes

Creatine Deficiency syndromes comprise three inherited disorders of creatine synthesis and transport. Two of them are inherited in an autosomal-recessive fashion and directly result from enzyme deficiencies of creatine biosynthesis, namely guanidinoacetate methyltransferase deficiency (due to mutation of GAMT gene on 19p13.3), and L-arginine-glycine amidinotransferase deficiency (due to mutation of AGAT gene on 15q15.3) [32, 33]. Both types cause deficiency of brain creatine, but the former additionally results

in the accumulation of guanidinoacetate acid (GAA), which has epileptogenic potential and is neurotoxic [33, 34]. The third is an X-linked disorder that results from a deficiency of the creatine transporter 1, which transports creatine intracellularly, and results from SLC6A8 gene mutation on Xq28 [32, 33, 35, 36]. These patients have normal body fluid levels of creatine with increased excretion [34].

The main function of creatine is to transfer high-energy groups from sites of production within the mitochondria to sites of energy consumption in the cytoplasm [32]. Individuals with brain creatine deficiency syndromes will present with developmental delay including speech and cognitive impairment, hypotonia, autism, seizures, and behavioral problems, [32, 34] with variations in the clinical presentation depending on the type of disorder. For individuals with AGAT deficiency, delays in development are more pronounced in speech, while patients with GAMT deficiency may have extrapyramidal movement disorders and be intractable [32, 34]. Males with creatine transporter deficiency in some cases may present with mid-facial hypoplasia and short stature [36].

Diagnostic workup involves serological and laboratory measurements of creatine in blood, urine, and cerebrospinal fluid with eventual genetic testing [33]. Structural MR imaging in many cases is normal [34, 37, 38]. In some cases, there is evidence of T2 hyperintensity within the basal ganglia [39–41], mildly decreased myelination, [34] periventricular T2 hyperintense signal, and cerebral atrophy [42]. Magnetic resonance spectroscopy has greater utility and typically demonstrates absent or markedly decreased creatine signal (Fig. 4) [33, 36, 37, 39, 40, 43]. Treatment changes with dietary restriction and creatine supplementation can also be tracked using MR spectroscopy. Creatine levels show improvement in the AGAT and GAMT subtypes, which typically are responsive to this type of therapy [32, 37, 39, 40, 43].

Vanishing White Matter Disease/Childhood Ataxia with Central Nervous System Hypomyelination

Vanishing white matter disease (VWM) is an autosomal-recessive leukoencephalopathy, primarily affecting children. Initial reports date back to 1962, in which Eicke described neuropathologic findings consistent with VWM [44]. However, it was not until 1993 and 1994 when Hanefeld et al. [45] and Schiffmann et al. [46] described the clinical entity and imaging findings in a series of 3 and 4 patients, respectively [47]. In 1997, van der Knapp et al. described imaging findings in a larger series of 9 patients and found that the MRI and MR spectroscopy findings were consistent with a progressive cystic degeneration of white matter, confirmed with autopsy [47, 48]. VWM is related to mutations in any of the five genes that encode for the eukaryotic translation initiation factor (*EIF2B 1-5*) [49].

The classic and most common phenotype is characterized by onset between the ages of 2 and 6 years [47] of a subacute or chronic progressive neurological deterioration composed of cerebellar ataxia, spasticity, and mild mental decline [45–48, 50]. It is often preceded by an initially normal or mildly delayed development and triggered or exacerbated by trauma, infection or fright [47, 51, 52]. Optic atrophy and epilepsy may develop [47, 53]. Other phenotypes have been described including antenatal/early-infantile forms (characterized by severe encephalopathy, oligohydramnios, intrauterine growth retardation, microcephaly, and decreased fetal movement), and late childhood/adult-onset forms (characterized by seizures, psychiatric symptoms, dementia, and motor deterioration) [47, 51].

Imaging is essential in diagnosis. On CT, there is diffuse symmetrical hypoattenuation of cerebral white matter [51]. On MR imaging, there is diffuse symmetrical involvement of cerebral white matter including the corpus callosum with extensive T1 hypointense, and T2/proton density hyperintense signal abnormalities (Fig. 5) [5, 45, 46, 51, 54]. The subcortical U fibers, basal ganglia, internal capsules, and external capsules are usually spared. Over time, there are areas of FLAIR hypointense signal corresponding to that of CSF surrounded by abnormally T2/FLAIR hyperintense white matter signal, representing areas of cystic degeneration or rarefaction [47, 50]. In advanced cases, CSF signal replaces large portions of the cerebral white matter, with disappearance of white matter occurring in a "melting away pattern" [47]. There may also be atrophy of the cerebellum and brainstem. On DWI, diffusion is restricted at the periphery, while it is facilitated in areas that have already progressed to cystic degeneration. There is no abnormal enhancement on contrast-enhanced imaging [47]. MR spectroscopy demonstrates a decrease in all metabolites except for lactate and glucose peaks, which are elevated in the affected areas [47, 50].

Adrenoleukodystrophy

Adrenoleukodystrophy (ALD) is an X-linked metabolic disorder caused by deficiency in peroxisomal enzyme, which results in the accumulation of very long-chain fatty acids (VLCFA) in plasma and tissues such as adrenal glands, testis, brain, and spinal cord [55]. It is caused by a mutation in *ABCD1* gene mapped by Xq28, which is the terminal segment of the long arm of the X chromosome. Accumulation of VLCFA in the brain causes progressive

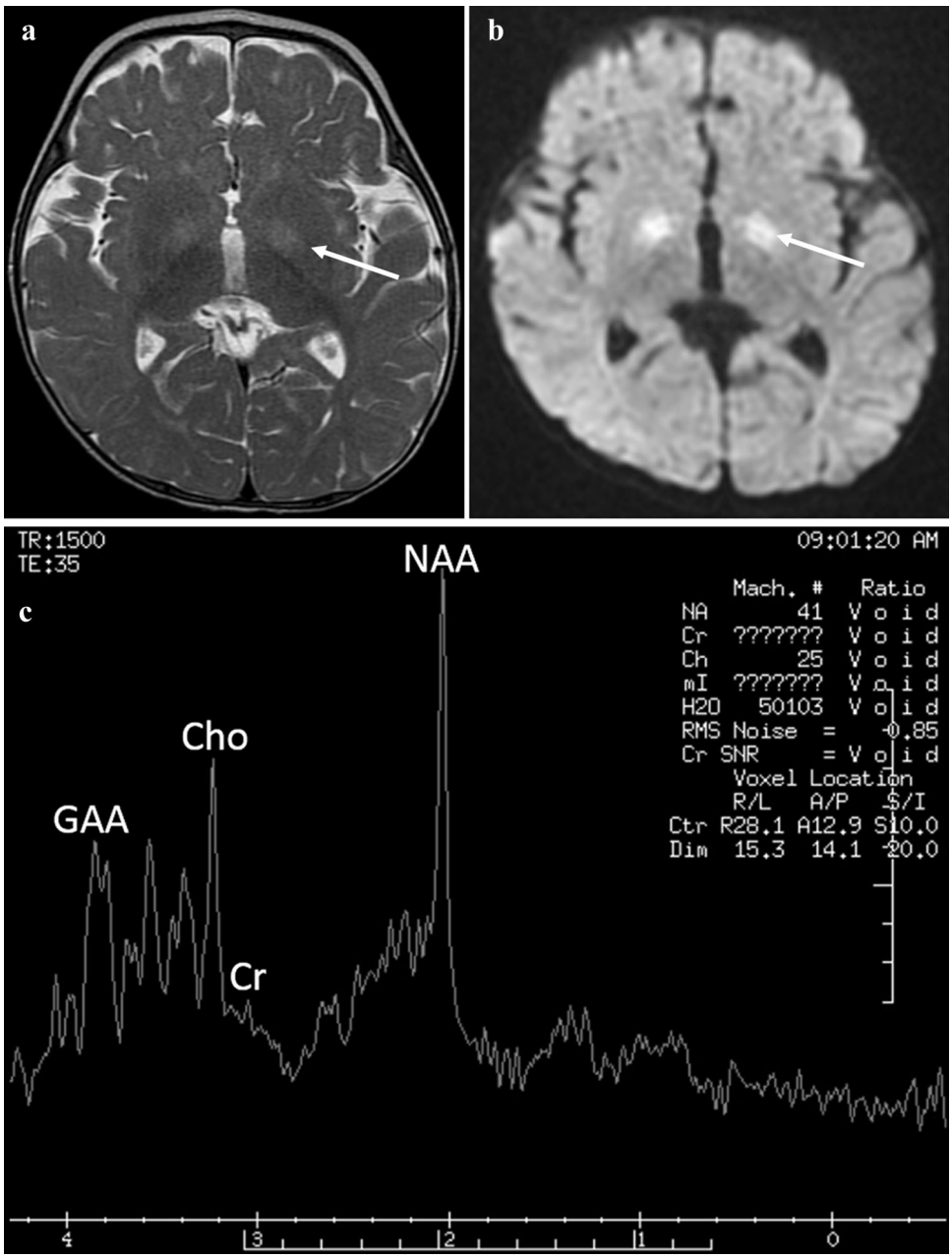

Fig. 4 Guanidinoacetate methyltransferase deficiency (GAMT), a subtype of creatine synthetase deficiency. The globus palladi are abnormal with increased signal on axial T2-weighted (**a**) and diffusion-weighted (**b**) images (*arrows*). No enhancement was identified on the post-contrast images (not shown). Spectroscopy with TE = 35 ms (**c**) shows no detectable creatine peak (Cr), also undetectable with long TE (not shown). In addition, the short TE sequence shows a broad guanidinoacetate peak at 3.78 ppm (GAA). The choline (Cho) and NAA peaks (NAA) are normal, and there are no abnormal lactate or lipid peaks

inflammatory demyelination resulting in severe neurocognitive disability, vegetative state, and death [56]. Several phenotypes of ADL have been described [55–58], including childhood (2.5–10 years), adolescent (10–21 years), and adult (>21 years) cerebral ALD, Adrenomyeloneuropathy (AMN) ± cerebral disease, Addison-only disease, and women with X-linked ALD [55].

Childhood cerebral ALD (CCALD), AMN, and Addison-only disease are the most prevalent phenotypes [55, 57, 58]. The CCALD phenotype typically has an insidious onset with visuospatial and visuomotor disturbance, attention deficit, and reasoning impairment. With progression, patients develop withdrawn or hyperactive behavior, apraxia, astereognosis, auditory impairment, decreased visual acuity, hemiparesis, spastic tetraparesis, and eventually become severely handicapped, bedridden requiring full-time nursing care and feeding tube. Adolescent and adult cerebral ALD phenotypes have a similar presentation, but with a slower course of cognitive decline and neuropsychiatric disturbance. Patients with AMN typically present in the 3rd or 4th decade with spastic paraparesis, sensory ataxia, with impaired vibration sense, urinary sphincter dysfunction, and impotence. Males that have the Addison-only phenotype typically present with adrenocortical insufficiency several years before onset of neurological symptoms. Majority of the phenotypes have a

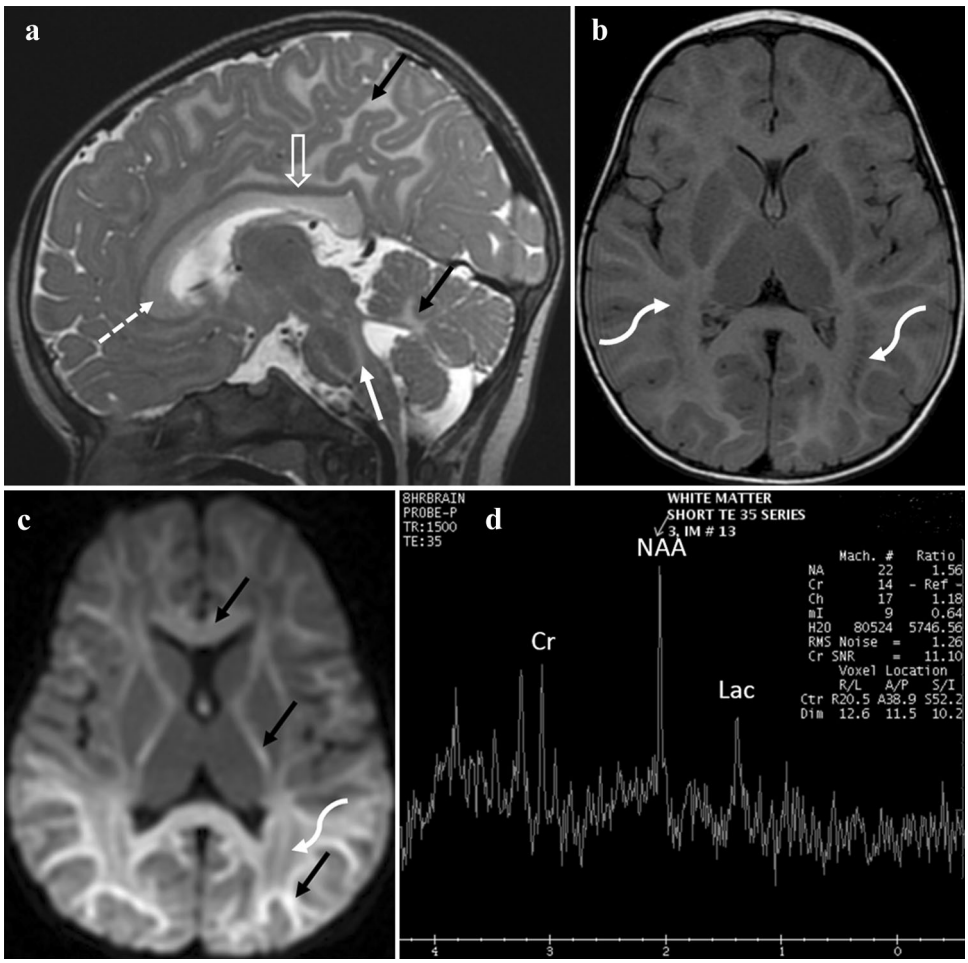

Fig. 5 Vanishing white matter disease. Sagittal T2-weighted image (**a**) shows homogeneous hyperintensity of cerebral and cerebellar white matter (*black arrows*), central tegmental tracts in the pontine tegmentum (*white arrow*), and involvement of the inner rim of the corpus callosum (*dashed arrow*). The outer rim of the corpus callosum is spared (*open arrow*). An axial T1-weighted image (**b**) shows linearly arrayed foci in the parieto-occipital white matter with signal intensity similar to CSF (*curved white arrows*), indicating frank cavitation. A corresponding axial diffusion-weighted image (**c**) shows cavitating areas (*curved white arrow*) as low signal intensity, while pre-cavitary affected white matter has extensive, marked hyperintensity indicating restricted diffusion (*black arrows*). MR spectroscopy with TE = 35 ms (**d**) is near normal early in the disease, except for subtle decrease in creatine at 3.0 ppm (Cr) and elevation of lactate at 1.3 ppm (Lac)

rapidly progressive course. Women with X-ALD have onset in the 4th or 5th decade of life with slower progression [55].

Neuroimaging is an important component of the workup. In majority of cases of cerebral ALD, there is initial involvement of the parieto-occipital deep white matter [58], and splenium of the corpus callosum [55, 59], although not infrequently lesions may begin in the genu of the corpus callosum, frontal white matter, and cerebellar white matter [59]. There is usually involvement of centrum semiovale, visual and auditory tracts including the geniculate bodies, internal capsules, and pyramidal tracts [55, 60], with relative sparing of the subcortical U fibers [58].

Affected areas show T1 hypointense and T2/FLAIR hyperintense signal without enhancement in the initial stages of the disease. As the disease progresses rapidly in many cases, lesions may enhance, reflecting severe inflammation and blood–brain barrier breakdown (Fig. 6). Enhancement typically affects the leading edge of the actively demyelinating white matter [60, 61]. In men with cerebral ALD and AMN, cerebral demyelination may spontaneously arrest, and the patient may remain stable for decades [55]. Severity of disease and treatment response can be tracked using an MR scoring system developed by Loes et al. [59]. MR spectroscopy typically demonstrates low NAA and elevated lactate and choline levels and can be used to track treatment response [62].

Patients affected with the AMN variant may have normal brain MRI or may show mild signal changes in the pyramidal tracts within the brainstem and internal capsule, reflecting Wallerian degeneration. These findings are, however, only considered cerebral ALD if signal abnormalities extend beyond the internal capsule and pyramidal tracts. MR imaging of the spinal cord in these patients shows nonspecific atrophy without demyelination or enhancement [55].

Alexander Disease

Alexander disease (AD) is a rare, primarily nonfamilial fibrinoid leukodystrophy characterized by the presence of Rosenthal fibers (i.e., eosinophilic, hyaline, and

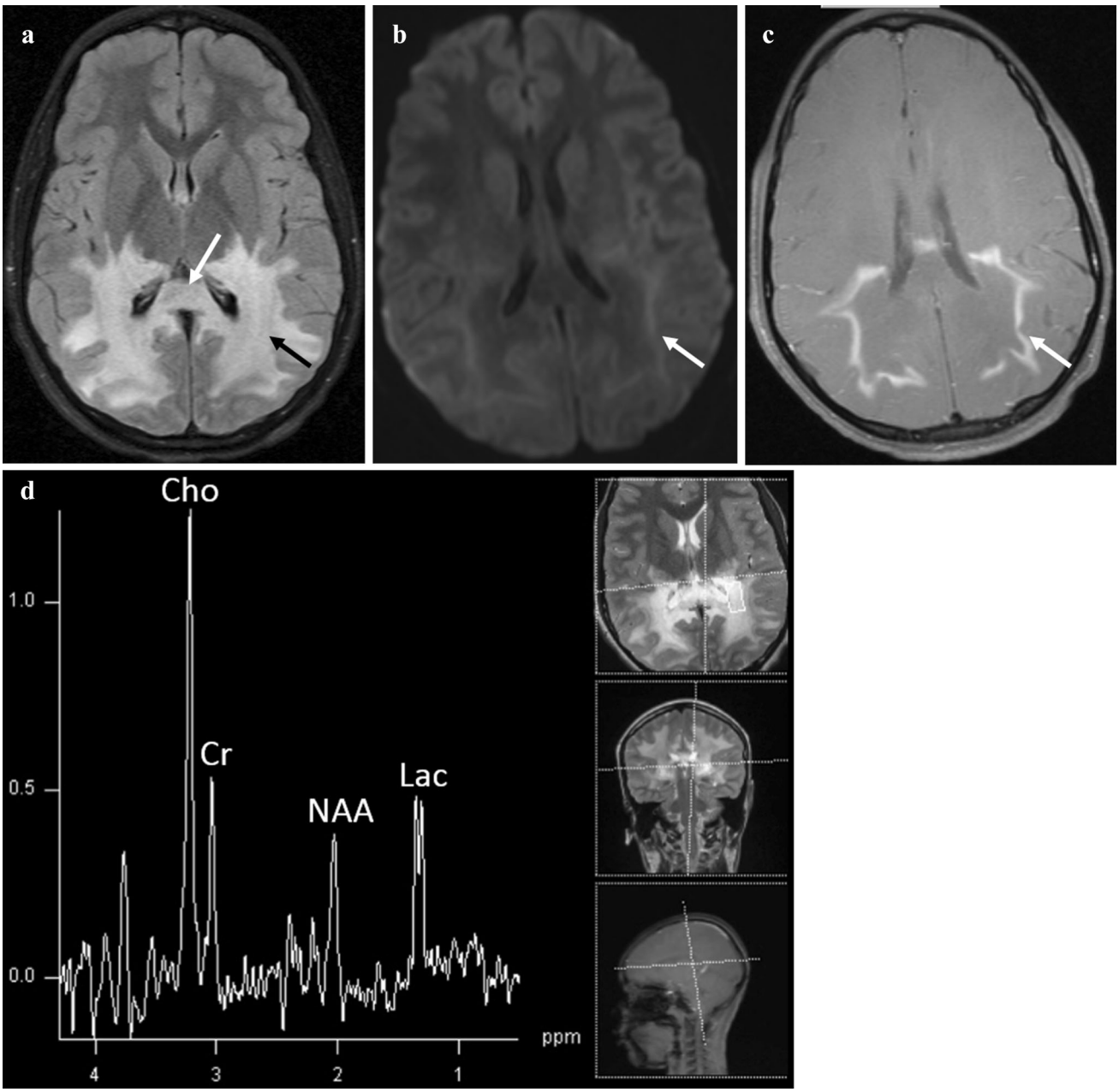

Fig. 6 Adrenoleukodystrophy. An axial FLAIR image (**a**) shows extensive symmetric T2 prolongation in the posterior supratentorial white matter bilaterally (*black arrow*) with involvement of the splenium of the corpus callosum (*white arrow*). Axial diffusion-weighted (**b**) and contrast-enhanced T1-weighted (**c**) images demonstrate marginal restricted diffusion and enhancement (*white arrows*). The posterior-predominant distribution of the signal abnormality as well as the "leading edge" diffusion and enhancement patterns are characteristic of adrenoleukodystrophy. MR spectroscopy with TE = 35 ms (**d**) shows a large lactate peak (Lac) in the affected white matter. NAA (NAA) and creatine (Cr) are abnormally low while the choline (Cho) is elevated. This is a nonspecific marker of parenchymal injury, but may be seen in the setting of inborn errors of metabolism

argyrophilic inclusions) [63] in astrocytes, and found to be caused by mutations in the gene encoding for glial fibrillary acidic protein (GFAP) [64]. Four subtypes of the AD have been described, namely, neonatal, infantile, juvenile, and adult forms with varied phenotypic expressions.

The neonatal form has a severe course with rapid progression. Affected individuals present with intractable seizures, hydrocephalus due to aqueductal stenosis, increased CSF protein content, severe motor and intellectual disability, and mortality within the first two years [65]. The infantile form is the most notable, and typically has onset by 6 months with variable expression. Affected individuals have progressive psychomotor retardation with loss of developmental milestones,

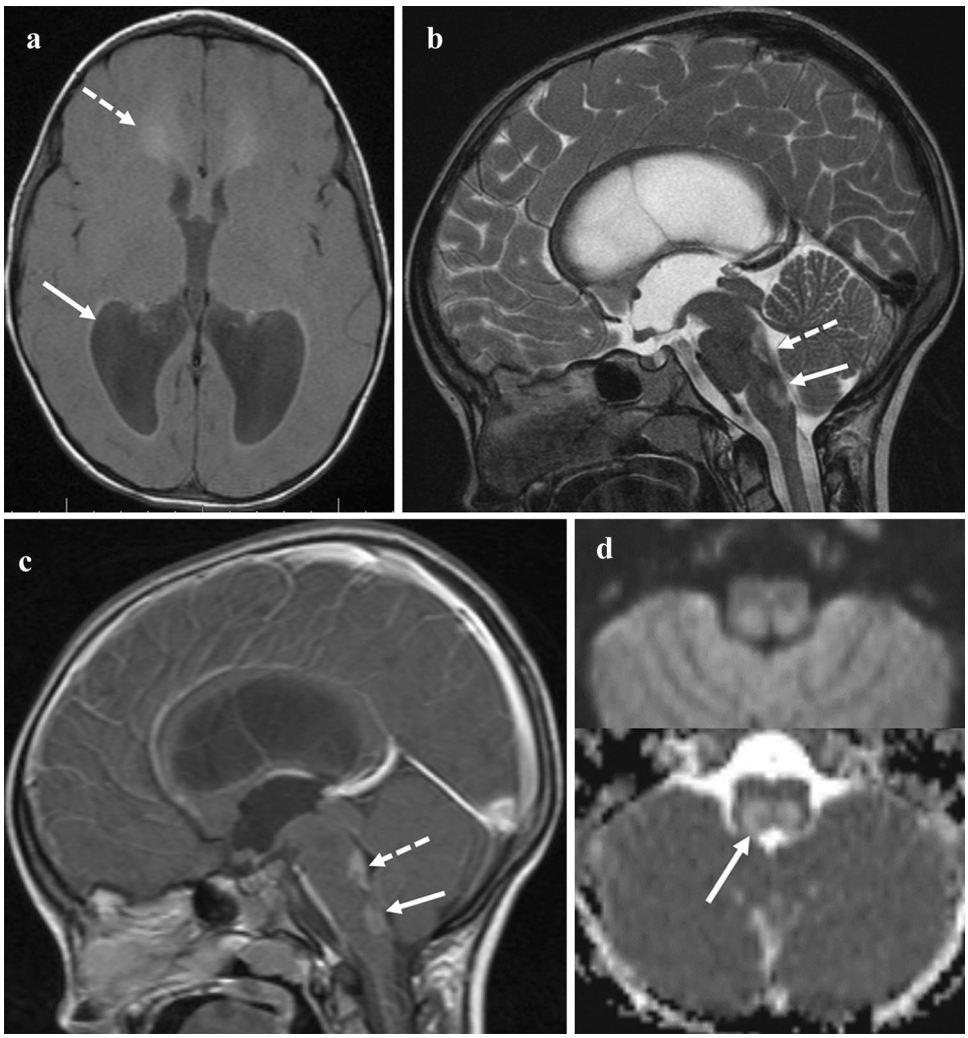

Fig. 7 Alexander disease (juvenile form). On this axial unenhanced T1-weighted image (**a**), there is marked enlargement of the lateral and third ventricles with normal-sized 4th ventricle consistent with obstructive hydrocephalus secondary to aqueductal stenosis. There is lateral ventricle ependymal hyperintensity (*arrow*) as well as periventricular white matter hyperintensity with frontal predominance (*dashed arrow*). The basal ganglia and thalami appear normal. A midline sagittal T2-weighted image (**b**) demonstrates symmetric T2 hyperintense lesions in the dorsal medulla (*arrow*) with smaller symmetric lesions seen in the dorsal pons (*dashed arrow*). The medulla appears enlarged. A corresponding sagittal contrast-enhanced T1-weighted image (**c**) shows enhancement of the dorsal medulla and pons lesions (same annotations). There was also subtle ependymal and periventricular white matter enhancement (not shown). A coned down axial ADC map (**d**) shows facilitated diffusion within the symmetric dorsal medulla lesions (*arrow*)

macrocephaly, severe seizures, spastic quadriparesis, hypereflexia, ataxia, and hydrocephalus [66–68].

The juvenile and adult forms have later onset and slower progression [67]. The former usually presents between the ages of 4 and 10 years, with survival extending to the adolescent and early adult years. Symptoms primarily include bulbar and pseudobulbar signs including swallowing, vomiting, and speech impairment as well as breathing difficulty due to brainstem involvement. Other symptoms include lower limb spasticity, ataxia, and gradual loss of intellect [66, 67]. The adult form is the most variable, but not infrequently resembles the juvenile form. Individuals present with pyramidal signs, ataxia, ocular motor abnormalities, autonomic disturbances, and palatal myoclonus together with bulbar and pseudobulbar signs [67, 69–71].

Although the definitive diagnosis is primarily by genetic testing, neuroimaging can be helpful. Based on a hallmark study by Van der Knaap, the typical MR findings include (i) extensive predominantly frontal white matter abnormalities including edema, atrophy, and cystic degeneration, (ii) T2 hypointense and T1 hyperintense periventricular rim, (iii) signal abnormalities in the basal ganglia and thalami, (iv) signal abnormalities in the brainstem, and (v) contrast enhancement involving one or more affected structures including ventricular lining, periventricular rim, optic chiasm, fornix, basal ganglia, thalamus, dentate nucleus, cerebellar cortex, and brainstem (Fig. 7). Four of the five criteria need to be met to make an MRI-based diagnosis [68, 72].

In the adult-onset form, progressive atrophy of the medulla and upper cervical cord with T2 hyperintense signal is felt to be highly suggestive [70, 71, 73], with supratentorial involvement and enhancement much less common in older adults [70, 71]. On MR spectroscopy, NAA is typically decreased or absent, [70, 74] distinguishing it from Canavan disease. Atypical MR findings include predominant or isolated posterior fossa involvement, multifocal tumor-like brainstem lesions, and diffuse signal involving brainstem and thalamus [72].

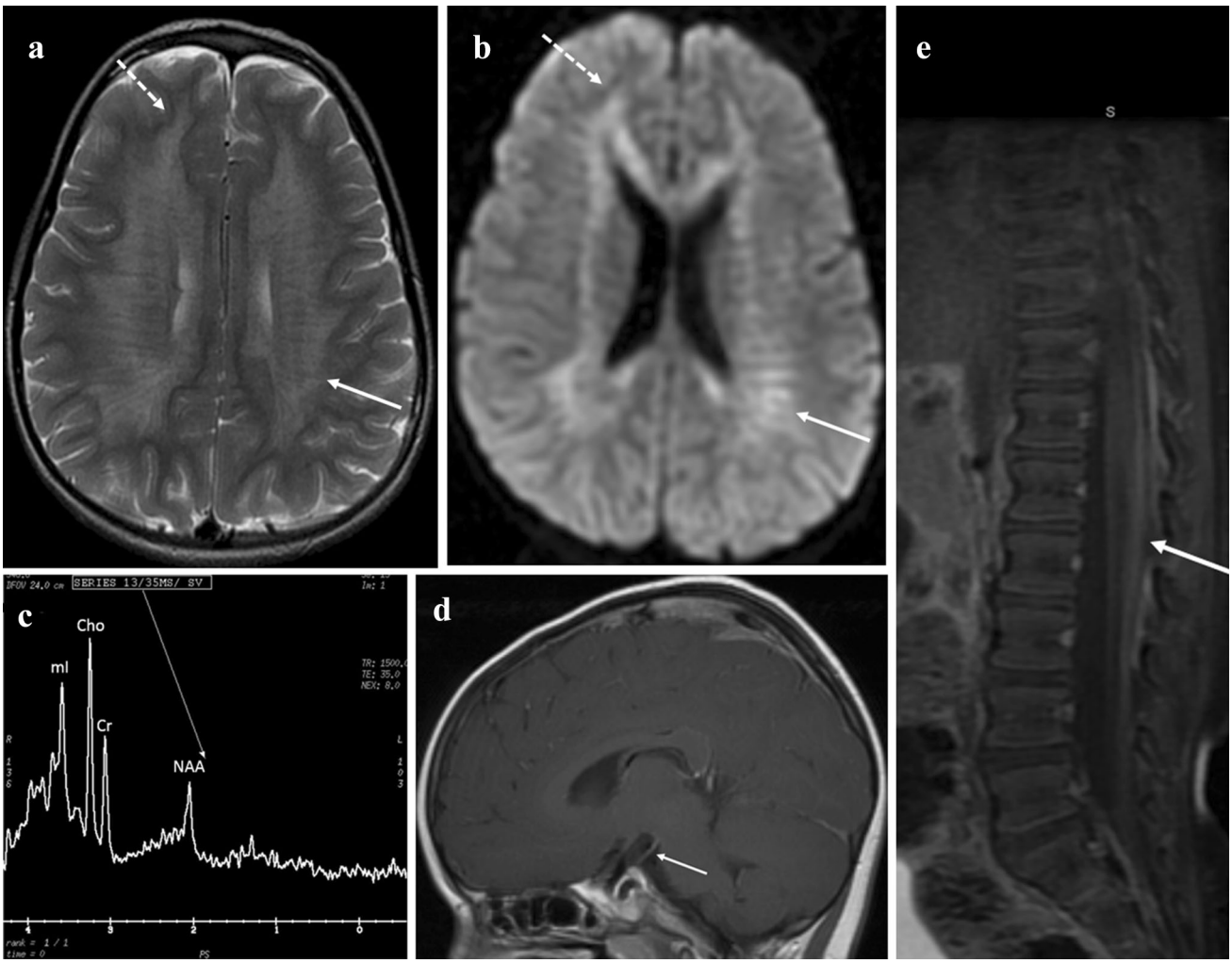

Fig. 8 Metachromatic leukodystrophy. Axial T2-weighted (**a**) and diffusion-weighted (**b**) images show diffusely increased signal in the periventricular and deep white matter extending from the lateral ventricles in the classic "tigroid" pattern (*arrows*). Note that the subcortical U fibers are spared (*dashed arrows*). No signal abnormality was seen in the cerebellum (not shown). MR spectroscopy with TE = 35 ms (**c**) in the areas of abnormal white matter shows elevation of myo-inositol at 3.5 ppm (mI) and marked decrease in NAA at 2.0 ppm (NAA). Creatine at 3.0 ppm (Cr) and choline at 3.2 ppm (Cho) are also labeled. Although there is no abnormal enhancement of the white matter, a paramedian sagittal T1-weighted image (**d**) of a different patient shows abnormal enhancement of the cisternal portion of the oculomotor nerves (*arrow*), likely due to the inflammatory response to myelin breakdown. A sagittal contrast-enhanced T1-weighted image of the lumbar spine (**e**) also shows enhancement of the cauda equina (*arrow*)

Metachromatic Leukodystrophy

Metachromatic leukodystrophy (MLD) is an inherited autosomal-recessive disorder resulting from lysosomal storage deficiency of arylsulfatase A [75]. Deficiency of arylsufatase A results in accumulation of galactosylceramide sulfate in the oligodendrocytes and Schwann cells leading to progressive demyelination within the central and peripheral nervous system [75–78]. This disease can be categorized into three subtypes based on onset of the disease, namely, late-infantile (1–2 years), juvenile (3–16 years), and adult (>16 years).

The late-infantile subtype is the most common form of MLD. Affected individuals may present with weakness and gait disturbance, ataxia, developmental delay, loss of speech, optic atrophy, and progressive spastic tetraplegia [79]. The juvenile subtype presents similarly with mental retardation, speech, bulbar, and motor disturbances including ataxia and tremors; however, the course is much more protracted [80]. The adult type also has a more protracted course and affected individuals may present with personality and mental status changes, often misdiagnosed as schizophrenia, bipolar disorder, or dementia [81].

Neuroimaging is routinely part of the workup and can be helpful in making a diagnosis. Affected areas usually involve the centrum semiovale and periventricular white matter particularly surrounding the atria and frontal horns [81], initially sparing of the subcortical U fibers in the early

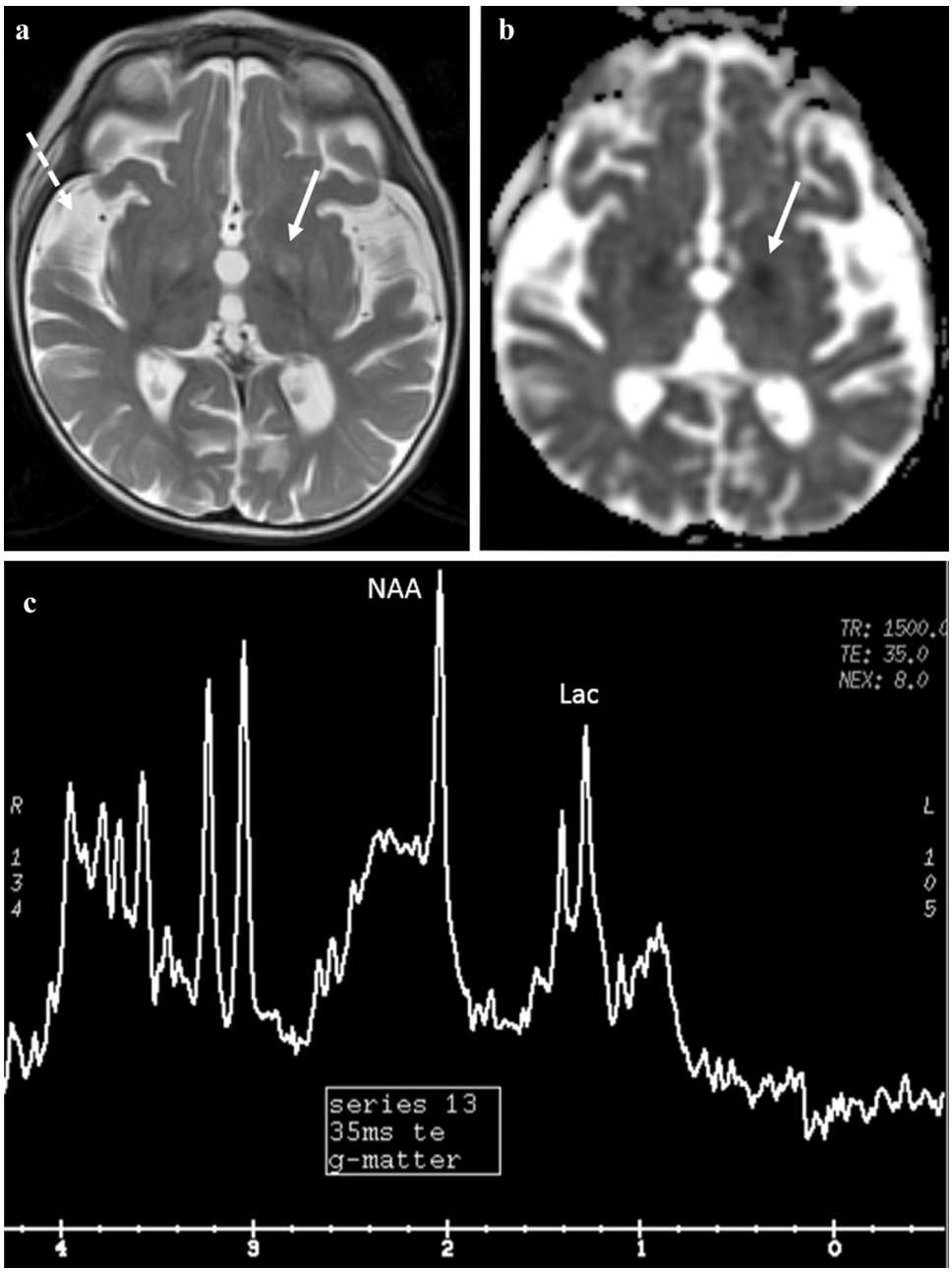

Fig. 9 Leigh disease. Axial T2-weighted image (**a**) and ADC map (**b**) through the basal ganglia demonstrate marked central and cortical volume loss with widening of the sulci (*dashed arrow*), with high T2 signal, and restricted diffusion in the globus pallidi (*arrows*). Signal abnormality also extended into the red nuclei and corticospinal tracts bilaterally (not shown). MR spectroscopy with TE = 35 ms (**c**), single voxel placed over right basal ganglia, shows a low NAA peak (NAA) and markedly elevated lactate doublet at 1.3 ppm (Lac)

stages [76, 82]. Disease progresses centrifugally and sometimes in a posterior to anterior fashion [76, 78, 82]. On T2-weighted MR imaging, there is symmetric diffuse high signal with a tigroid or leopard skin appearance [82, 83], indicative of advanced disease [77], which has also been described in Pelizaeus–Merzbacher disease (Fig. 8) [76, 82]. The tigroid appearance is created by the presence of unaffected perivascular spaces intervening in areas of demyelinated white matter [84].

On DWI, active areas of involvement may show restricted diffusion due to intermediate grade myelin cytotoxic edema [78, 85, 86]. Frequently, there is involvement of the corpus callosum, internal capsule, and the corticospinal tracts [76, 77]. There is no enhancement of the white matter lesions, although linear and punctate enhancement of intervening normal white matter [76] and multiple cranial nerve enhancement [87] have been reported. As the disease progresses, there is cortical atrophy with ventricular enlargement, and involvement of the subcortical U fibers and cerebellar white matter [77, 79, 81, 82]. On MR spectroscopy, elevation of choline indicating myelin turnover, myo-inositol indicating reactive gliosis, and reduced NAA/creatine ratio indicating neuronal loss have been reported [86]. A scoring system for

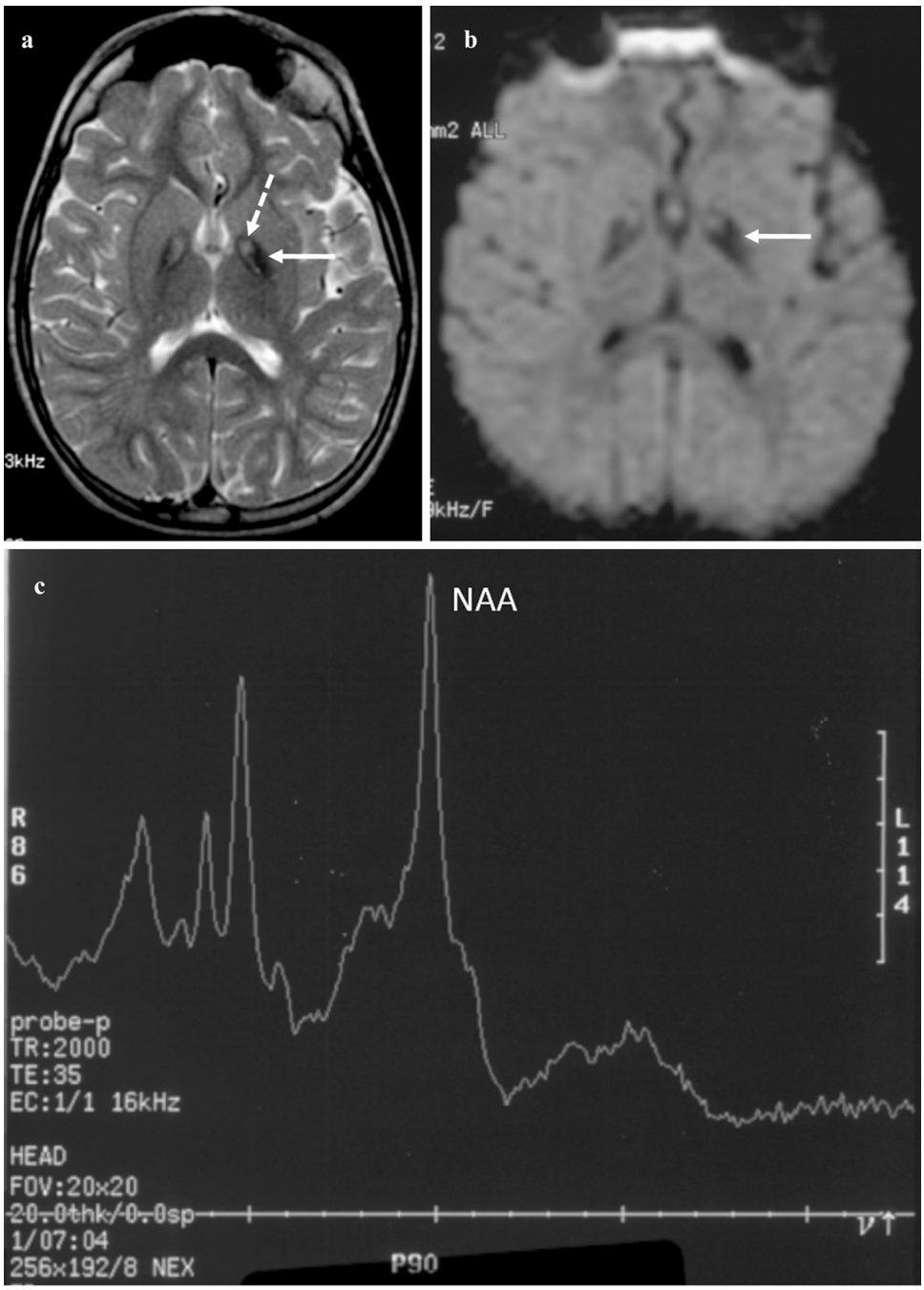

Fig. 10 Pantothenate kinase-associated neurodegeneration. Axial T2-weighted (**a**) and diffusion-weighted (**b**) images show the typical "eye of the tiger" sign, with marked hypointensity of the globus pallidi (*arrows*) with a small hyperintense area (*dashed arrow*) in the anteromedial part of the nuclei. The globus pallidi were hyperintense on T1-weighted images (not shown), corresponding to the regions of T2 hypointensity. MR spectroscopy with TE = 35 ms (**c**) shows nonspecific mildly decreased NAA in the globus pallidus indicating neuronal loss (NAA)

disease severity may be used to categorize patients into mild, moderate, or severe disease groups based on imaging characteristics [77].

Leigh Syndrome (Subacute Necrotizing Encephalomyelopathy)

Leigh syndrome (LS) is an inherited mitochondrial disorder with progressive neurodegenerative and metabolic disturbance of infancy and early childhood [88]. Its pathogenesis has been related to autosomal-recessive inheritance of mutations in mitochondrial proteins or X-linked inheritance of mutations in the *PDHA1* gene that codes for pyruvate dehydrogenase [90]. The onset of the disease typically occurs between 3 and 12 months of age with eventual death by 2 years of age; however, later onset (juvenile onset) and slower progression have also been reported [90, 91].

The clinical presentation of LS is variable and may include psychomotor delay or regression, cognitive decline, hypotonia, movement disturbances including

dyskinesia, akinesia, dystonia, ataxia, and brainstem abnormalities including respiratory dysfunction, ocular movement abnormalities, lactic acidosis, and disordered thermoregulation [90, 92]. Respiratory failure is reported to be the most common cause of death [93, 94].

In addition to biochemical testing, which demonstrates elevation in lactate and pyruvate in the CSF and blood, neuroimaging with spectroscopy can be helpful. Affected individuals typically have symmetrical lesions in one or more areas of the brain, including the basal ganglia particularly the putamen and globus pallidus, thalami, subthalamic nuclei, midbrain, pons, cerebellum, and spinal cord [90, 92, 95, 96]. Lesions in the lower brainstem tend to be more common in the later stages of the disease [93].

Affected areas of the brain typically show low attenuation on CT, hyperintense signal on T2-weighted imaging, and hypointense signal on T1-weighted imaging (Fig. 9) [90]. Involvement of the bilateral brainstem and basal ganglia is included in the diagnostic criteria for LS. However, the lack of a visible lesion in a patient with clinical findings for LS does not exclude the disease. Acute lesions may show restricted diffusion on diffusion-weighted imaging [96]. Affected patients may also demonstrate elevated lactate and choline levels on MR spectroscopy in affected areas, but decreased NAA levels in regions of encephalomalacia [89•, 96]. Lesions may evolve over time with some lesions disappearing in response to treatment.

Pantothenate Kinase-Associated Neurodegeneration (PKAN) (Formerly Known as Hallervorden–Spatz Syndrome)

Pantothenate kinase-associated neurodegeneration (PKAN) is an autosomal-recessive disorder due to a mutation in the PANK2 gene on chromosome 20p12.3–p13, which leads to mitochondrial Co-enzyme A deficiency [97–99]. It is characterized by progressive extrapyramidal dysfunction due to abnormal brain iron deposition.

There are two known phenotypes of PKAN termed classical and atypical forms [3••]. Affected individuals presenting with the classical form have early onset usually the first decade of life, fast progression, and retinal degeneration. In the atypical form, onset is late, usually the second or third decade of life with slow progression, prominent speech impairment, intelligence decline, and neuropsychiatric symptoms [100]. In both phenotypes, there is evidence of extrapyramidal dysfunction, which may be characterized by tremors, bradykinesia, dystonia, rigidity, choreoathetosis, and spasticity [97–100].

MR imaging features are characterized by susceptibility signal on gradient-recalled echo sequences due to iron deposition in the globus pallidi and substantia nigra. On T2-weighted and FLAIR imaging, there is hypointense signal in the globus pallidi with central anteromedial T2 hyperintensity creating the so-called "eye of a tiger" appearance or sign, which is pathognomonic for PKAN (Fig. 10). No restricted diffusion is seen, and there is no role for contrast administration [100, 101]. On MR spectroscopy, there is a decrease in NAA and reduced NAA/creatine ratio secondary to neuronal loss [98].

Differential considerations for PKAN include HARP syndrome (Hypopre-B-lipoproteinemia, Acanthocytosis, Retinitis pigmentosa, and Pallidal degeneration) which is known to be allelic to PKAN [99], neuroferritinopathy, aceruloplasminemia, [100] and SENDA disease (static encephalopathy with neurodegeneration in childhood) [5•].

Conclusions

Pediatric metabolic brain disorders are a varied group of diseases that cause progressive brain injury, often preferentially targeting the white matter, deep gray nuclei, and brainstem. Brain MRI plays a pivotal role in diagnosing these disorders and can be used to follow progression and treatment response. By incorporating DWI and MR spectroscopy findings, the radiologist can provide a more targeting differential diagnosis.

Compliance with Ethics Guidelines

Human and Animal Rights and Informed Consent This article does not contain any studies with human or animal subjects performed by any of the authors.

Conflict of Interest Kofi-Buaku Atsina and Vinay V. R. Kandula each declare no potential conflicts of interest. Lauren W. Averill is a section editor for *Current Radiology Reports.*

References

Recently published papers of particular interest have been highlighted as follows:
- • Of importance
- •• Of major importance

1. Menkes JH, Hurst PL, Craig JM. A new syndrome: progressive familial infantile cerebral dysfunction associated with an unusual urinary substance. Pediatrics. 1954;14:452–67.
2. Strauss KA, Puffenberger EG, Morton DH. Maple syrup urine disease. Seattle: University of Washington; 1993.
3. •• Patay Z, Blaser SI, Poretti A et al. Neurometabolic diseases of childhood. Pediatr Radiol (2015);45 (Suppl 3): S473–S484. *Neurometabolic diseases are subdivided in various groups depending on the predominantly involved tissue, the involved metabolic processes and primary age of the child at presentation with comprehensive tabulation of selected disorders.*

4. Puffenberger EG. Genetic heritage of the old order mennonites of Southeastern Pennsylvania. Am J Med Genet. 2003;121C:18–31.
5. Carleton SM, Peck DS, Grasela J, et al. DNA carrier testing and newborn screening for maple syrup urine disease in old order mennonite communities. Genet Test Mol Biomark. 2010;14:205–8.
6. Morton DH, Strauss KA, Robinson DL, et al. Diagnosis and treatment of maple syrup disease: a study of 36 patients. Pediatrics. 2002;109:999–1008.
7. Chuang JL, Davie JR, Chinsky JM, et al. Molecular and biochemical basis of intermediate maple syrup urine disease. Occurrence of homozygous G245R and F364C mutations at the E1 alpha locus of Hispanic-Mexican patients. J Clin Invest. 1995;95:954–63.
8. Indiran V, Gunaseelan RE. Neuroradiological findings in maple syrup urine disease. J Pediatr Neurosci. 2013;8:31–3.
9. Jain A, Jagdeesh K, Mane R, et al. Imaging in classic form of maple syrup urine disease: a rare metabolic central nervous system. J Clin Neonatol. 2013;2:98–100.
10. Cavalleri F, Berardi A, Burlina A, et al. Diffusion-weighted MRI of maple syrup urine disease encephalopathy. Neuroradiology. 2002;44:499–502.
11. Jan W, Zimmerman RA, Wang ZJ, et al. MR diffusion imaging and MR spectroscopy of maple syrup urine disease during acute metabolic decompensation. Neuroradiology. 2003;45:393–9.
12. Applegarth DA, Toone JR. Nonketotic hyperglycinemia (glycine encephalopathy): laboratory diagnosis. Mol Genet Metab. 2001;74:139–46.
13. Kanekar S, Byler D. Characteristic MRI findings in neonatal nonketotic hyperglycinemia due to sequence changes in GLDC gene encoding the enzyme glycine decarboxylase. Metab Brain Dis. 2013;28:717–20.
14. Hoover-Fong JE, Shah S, Van Hove JLK, et al. Natural history of nonketotic hyperglycinemia in 65 patients. Neurology. 2004;63:1847–53.
15. • Poretti A, Blaser SI, Lequin MH, et al. Neonatal neuroimaging findings in inborn errors of metabolism. J Magn Reson Imaging 2013;37:294–312. *The authors of the above article provide imaging findings of a broader spectrum of pediatric metabolic disorders beyond the scope of our article.*
16. Press GA, Barshop BA, Haas RH, et al. Abnormalities of the brain in nonketotic hyperglycinemia: MR manifestations. Am J Neuroradiol. 1989;10:315–21.
17. Agamanolis DP, Potter JL, Herrick MK, et al. The neuropathology of glycine encephalopathy: a report of five cases with immunohistochemical and ultrastructural observations. Neurology. 1982;32:975–85.
18. Mourmans J, Majoie CBLM, Barth PG, et al. Sequential MR imaging changes in nonketotic hyperglycinemia. Am J Neuroradiol. 2006;27:208–11.
19. Gerritsen T, Kaveggia E, Waisman HA. A new type of hyperglycinemia with hyperoxaluria. Pediatrics. 1965;36:882.
20. Shah DK, Tingay DG, Fink AM, et al. Magnetic resonance imaging in neonatal nonketotic hyperglycinemia. Pediatr Neurol. 2005;33(1):50–2.
21. Viola A, Chabrol B, Nicoli F, et al. Magnetic resonance spectroscopy study of glycine pathways in nonketotic hyperglycinemia. Pediatr Res. 2002;52:292–300.
22. Huisman T, Thiel T, Steinmann B, et al. Proton magnetic resonance spectroscopy of the brain of a neonate with nonketotic hyperglycinemia: in vivo–in vitro (ex vivo) correlation. Eur Radiol. 2002;12:858–61.
23. Chung W-S, Chao M-C, Lin F-J, et al. Magnetic resonance findings in an infant with nonketotic hyperglycinemia. J Radiol Sci. 2011;36:177–81.
24. Traeger EC, Rapin I. The clinical course of Canavan disease. Pediatr Neurol. 1998;18:207–12.
25. Namboodiri AM, Peethambaran A, Mathew R, et al. Canavan disease and the role of N-acetylaspartate in myelin synthesis. Mol Cell Endocrinol. 2006;252:216–23.
26. Merrill ST, Nelson GR, Longo N, et al. Cytotoxic edema and diffusion restriction as an early pathoradiologic marker in canavan disease: case report and review of the literature. Orphanet J Rare Dis. 2016;11:169.
27. McAdams H, Geyer C, Done S, et al. Canavan disease: CT and MR imaging of the brain. AJNR AmJNeuroradiol. 1990;11:805–10.
28. Cakmakci H, Pekcevik Y, Yis U, et al. Diagnostic value of proton MR spectroscopy and diffusion-weighted MR imaging in childhood inherited neurometabolic brain diseases and review of the literature. Eur J Radiol. 2010;74:e161–71.
29. Cheon J-E, Kim I-O, Hwang YS, et al. Leukodystrophy in children: a pictorial review of MR imaging features. RadioGraphics. 2002;22:461–76.
30. •• Ibrahim M, Parmar HA, Hoefling N, et al. Inborn errors of metabolism: combining clinical and radiologic clues to solve the mystery. Am J Roentgenol 2014;202:W315–27. *Pediatric metabolic disease can be challenging to diagnose because of the wide spectrum and overlap of clinical and radiologic findings. The authors of this article provide a systematic approach that employs categorizing these diseases into groups according to the extent of white matter and grey matter involvement, hypomyelination versus dysmyelination disorders, and lobar versus deep white matter involvement. Together with the clinical information, this approach can be helpful to the radiologist in narrowing down the differential diagnosis and ultimately in making the appropriate diagnosis.*
31. Karimzadeh P, Jafari N, Nejad Biglari H, et al. The clinical features and diagnosis of Canavan's disease : a case series of iranian patients. Iran J child Neurol. 2014;8:66–71.
32. Longo N, Ardon O, Vanzo R, et al. Disorders of creatine transport and metabolism. Am J Med Genet Part C. 2011;157:72–8.
33. Leuzzi V, Mastrangelo M, Battini R, et al. Inborn errors of creatine metabolism and epilepsy. Epilepsia. 2013;54:217–27.
34. Bianchi MC, Tosetti M, Battini R, et al. Treatment monitoring of brain creatine deficiency syndromes: A 1H- and 31P-MR spectroscopy study. Am J Neuroradiol. 2007;28:548–54.
35. Ardon O, Procter M, Mao R, et al. Creatine transporter deficiency: Novel mutations and functional studies. Mol Genet Metab Reports. 2016;8:20–3.
36. Salomons GS, Van Dooren SJM, Verhoeven NM, et al. X-linked creatine-transporter gene (SLC6A8) defect : a new creatine-deficiency syndrome. Am J Hum Genet. 2001;68(6):1497–500.
37. Bianchi MC, Tosetti M, Fornai F, et al. Reversible brain creatine deficiency in two sisters with normal blood creatine level. Ann Neurol. 2000;47:511–3.
38. Schulze A, Bachert P, Schlemmer H, et al. Lack of creatine in muscle and brain in an adult with GAMT deficiency. Ann Neurol. 2003;53:248–51.
39. Stöckler S, Holzbach U, Hanefeld F, et al. Creatine deficiency in the brain: a new, treatable inborn error of metabolism. Pediatr Res. 1994;36:409–13.
40. Ganesan V, Johnson A, Connelly A, et al. Guanidinoacetate methyltransferase deficiency: new clinical features. Pediatr Neurol. 1997;17:155–7.
41. Stockler-Ipsiroglu S, van Karnebeek C, Longo N, et al. Guanidinoacetate methyltransferase (GAMT) deficiency: outcomes in 48 individuals and recommendations for diagnosis, treatment and monitoring. Mol Genet Metab. 2014;111:16–25.

42. DeGrauw TJ, Salomons GS, Cecil KM, et al. Congenital creatine transporter deficiency. Neuropediatrics. 2002;33:232–8.
43. Declan O, Ryan S, Gajja S, et al. Guanidinoacetate methyltransferase (GAMT) deficiency: late onset of movement disorder and preserved expressive language. Dev Med Child Neurol. 2009;51(5):404–7.
44. Eicke W-J. Polycystische Umwandlung des Marklagers mit progredientem Verlauf. Arch für Psychiatr und Nervenkrankheiten Ver mit Zeitschrift für die Gesamte Neurol und Psychiatr. 1962;203:599–609.
45. Hanefeld F, Holzbach U, Kruse B, et al. Diffuse white matter disease in three children: an encephalopathy with unique features on magnetic resonance imaging and proton magnetic resonance spectroscopy. Neuropediatrics. 1993;24:244–8.
46. Schiffmann R, Moller JR, Trapp BD, et al. Childhood Ataxia with Diffuse Central Nervous System Hypomyelination. 1994. [Epub ahead of print].
47. van der Knaap MS, Pronk JC, Scheper GC. Vanishing white matter disease. Lancet Neurol. 2006;5:413–23.
48. van der Knaap MS, Barth PG, Gabreëls FJ, et al. A new leukoencephalopathy with vanishing white matter. Neurology. 1997;48:845–55.
49. Fogli A, Dionisi-Vici C, Deodato F, et al. A severe variant of childhood ataxia with central hypomyelination/vanishing white matter leukoencephalopathy related to EIF21B5 mutation. Neurology. 2002;59:1966–8.
50. Şenol U, Haspolat S, Karaali K, et al. Case report: MR imaging of vanishing white matter. AJR Am J Roentgenol. 2000;175:826–8.
51. Schiffmann R, Fogli A, van der Knaap MS, et al. Childhood ataxia with central nervous system hypomyelination/vanishing white matter. Seattle: University of Washington; 2003.
52. Vermeulen G, Seidl R, Mercimek-Mahmutoglu S, et al. Fright is a provoking factor in vanishing white matter disease. Ann Neurol. 2005;57:560–3.
53. Schiffmann R, Moller JR, Trapp BD, et al. Childhood Ataxia with D&s central nervous system hypomyelination. 1994. [Epub ahead of print].
54. van der Voorn JP, Pouwels PJW, Hart AAM, et al. Childhood white matter disorders: quantitative MR imaging and spectroscopy. Radiology. 2006;241:510–7.
55. Engelen M, Kemp S, de Visser M, et al. X-linked adrenoleukodystrophy (X-ALD): clinical presentation and guidelines for diagnosis, follow-up and management. Orphanet J Rare Dis. 2012;7:51.
56. Kemp S, Berger J, Aubourg P. X-linked adrenoleukodystrophy: clinical, metabolic, genetic and pathophysiological aspects. Biochim Biophys Acta. 2012;1822:1465–74.
57. Moser HW. Adrenoleukodystrophy: phenotype, genetics, pathogenesis and therapy. Brain. 1997;120:1485–508.
58. Kim JH, Kim HJ. Childhood X-linked adrenoleukodystrophy: clinical-pathologic overview and MR imaging manifestations at initial evaluation and follow-up. RadioGraphics. 2005;25:619–31.
59. Loes DJ, Hite S, Moser H, et al. Adrenoleukodystrophy: a scoring method for brain MR observations. Am J Neuroradiol. 1994;15:1761–6.
60. Patel PJ, Kolawole TM, Malabarey TM, et al. Pediatric radiology adrenoleukodystrophy: CT and MRI findings. 1995;25:256–8.
61. Melhem ER, Loes DJ, Georgiades CS, et al. X-linked adrenoleukodystrophy: The role of contrast-enhanced MR imaging in predicting disease progression. Am J Neuroradiol. 2000;21:839–44.
62. Rajanayagam V, Grad J, Krivit W, et al. Proton MR spectroscopy of childhood adrenoleukodystrophy. Am J Neuroradiol. 1996;17:1013–24.
63. Sawaishi Y. Review of Alexander disease: Beyond the classical concept of leukodystrophy. Brain Dev. 2009;31:493–8.
64. Brenner M, Johnson AB, Boespflug-Tanguy O, et al. Mutations in GFAP, encoding glial fibrillary acidic protein, are associated with Alexander disease. Nat Genet. 2001;27:117–20.
65. Springer S, Erlewein R, Naegele T, et al. Alexander disease—classification revisited and isolation of a neonatal form. Neuropediatrics. 2000;31:86–92.
66. Pridmore CL, Baraitser M, Harding B, et al. Alexander's disease : clues to diagnosis. J Child Neurol. 1993;8:134–44.
67. Messing A, Goldman J, Johnson A, et al. Alexander disease: new insights from genetics. J Neuropathol Exp Neurol. 2001;60:563–73.
68. Van der Knaap MS, Naidu S, Breiter SN, et al. Alexander disease: diagnosis with MR imaging. Am J Neuroradiol. 2001;22:541–52.
69. Balbi P, Salvini S, Fundarò C, et al. The clinical spectrum of late-onset alexander disease a systematic literature review. J Neurol 2010;257:1955–2.
70. Farina L, Pareyson D, Minati L, et al. Can MR imaging diagnose adult-onset Alexander disease? Am J Neuroradiol. 2008;29:1190–6.
71. Pareyson D, Fancellu R, Mariotti C, et al. Adult-onset Alexander disease: a series of eleven unrelated cases with review of the literature. Brain. 2008;131:2321–31.
72. Van Der Knaap MS, Salomons GS, Li R, et al. Unusual variants of Alexander's disease. Ann Neurol. 2005;57:327–38.
73. Schmidt H, Kretzschmar B, Lingor P, et al. Acute onset of adult Alexander disease. J Neurol Sci. 2013;331:152–4.
74. Muralidharan CG, Tomar RPS, Aggarwal R. MRI diagnosis of Alexander disease. South African J Radiol. 2012;16:116–7.
75. Andreas P, Fluharty AL, Fluharty CB, et al. Molecular basis of different forms of metachromatic leukodystrophy. N Engl J Med. 1991;324:18–22.
76. Kim TS, Kim IO, Kim WS, et al. MR of childhood metachromatic leukodystrophy. Am J Neuroradiol. 1997;18:733–8.
77. Eichler F, Grodd W, Grant E, et al. Metachromatic leukodystrophy: A scoring system for brain MR imaging observations. Am J Neuroradiol. 2009;30:1893–7.
78. Patay Z. Diffusion-weighted MR imaging in leukodystrophies. Eur Radiol. 2005;15:2284–303.
79. Zafeiriou DI, Kontopoulos EE, Michelakakis HM, et al. Neurophysiology and MRI in late-infantile metachromatic leukodystrophy. Pediatr Neurol. 1999;21:843–6.
80. Haltia T, Palo J, Haltia M, et al. Juvenile metachromatic leukodystrophy. Arch Neurol. 1980;37:42–6.
81. Waltz G, Harik SI, Kaufman B. Adult metachromatic leukodystrophy: value of computed tomographic scanning and magnetic resonance imaging of the brain. Arch Neurol. 1987;44:225–7.
82. Faerber EN, Melvin JJ, Smergel EM. MRI appearances of metachromatic leukodystrophy. Pediatr Radiol. 1999;29:669–72.
83. Reider-Grosswasser I, Bornstein N. CT and MRI in late-onset metachromatic leukodystrophy. Acta Neurol Scand. 1987;75:64–9.
84. Van Der Voorn JP, Pouwels PJW, Kamphorst W, et al. Histopathologic correlates of radial stripes on MR images in lysosomal storage disorders. Am J Neuroradiol. 2005;26:442–6.
85. Sener RN. Metachromatic leukodystrophy: diffusion MR imaging findings. AJNR Am J Neuroradiol. 2002;23:1424–6.

86. Sener RN. Metachromatic Leukodystrophy. Diffusion MR imaging and proton MR spectroscopy. Acta Radiol. 2003;44:440–3.
87. Maia ACM, Da Rocha AJ, Da Silva CJ, et al. Multiple cranial nerve enhancement: a new MR imaging finding in metachromatic leukodystrophy. Am J Neuroradiol. 2007;28:999.
88. Ashrafi M, Ghofrani M, Ghojevand N. Leigh synrome: clinical and paraclinical study. Acta Med Iran. 2002;40:236–40.
89. • Bray MD, Mullins ME. Metabolic white matter diseases and the utility of MR spectroscopy. Radiol Clin North Am 2014;52:403–11. *An easy-to read article by these authors provides background information on Magnetic resonance spectroscopy and its utility in aiding the diagnosis of metabolic white matter diseases.*
90. Sofou K, De Coo IFM, Isohanni P, et al. A multicenter study on Leigh syndrome: disease course and predictors of survival. Orphanet J Rare Dis. 2014;9:52.
91. Van Meir EG, Hadjipanayis CG, Norden AD, et al. Exciting new advances in neuro-oncology: the avenue to a cure for malignant glioma. CA A Cancer J Clin. 2010;60:166–93.
92. Lee H-F, Tsai C-R, Chi C-S, et al. Leigh syndrome: clinical and neuroimaging follow-up. Pediatr Neurol. 2009;40:88–93.
93. Arii J, Tanabe Y. Leigh syndrome: serial MR imaging and clinical follow-up. AJNR Am J Neuroradiol. 2000;21:1502–9.
94. Martin E, Burger R, Wiestler O, et al. Pediatric Radiology Short reports Brainstem lesion revealed by MRI in a case of Leigh' s disease with respiratory failure. Pediatr Radiol. 1990;20:349–50.
95. Farina L, Chiapparini L, Uziel G, et al. MR findings in Leigh syndrome with COX deficiency and SURF-1 mutations. Am J Neuroradiol. 2002;23:1095–100.
96. Bonfante E, Koenig MK, Adejumo RB, et al. The neuroimaging of Leigh syndrome: case series and review of the literature. Pediatr Radiol. 2016;46:443–51.
97. Parmar A, Khare S, Srivastav V. Pantothenate—kinase associated neurodegeneration. JAPU. 2012;60:74–6.
98. Hakim A, Rozeik C, Fedorcak M. Pantothenate kinase-associated neurodegeneration (PKAN) in a child with Down syndrome. A case report and follow-up with MRI. BJR Case Rep 2015:1–3.
99. Thomas M, Hayflick SJ, Jankovic J. Clinical heterogeneity of neurodegeneration with brain iron accumulation (Hallervorden-Spatz syndrome) and pantothenate. Mov Disord. 2004;19:36–42.
100. Hashemi H, Rokni Y, Adibi A. Atypical pantothenate-kinase associated neurodegeneration. Iran J Radiol. 2008;5:87–91.
101. Kruer M, Boddaert N, Schneider S, et al. Neuroimaging features of neurodegeneration with brain iron accumulation. AJNR AmJNeuroradiol. 2012;33:407–14.